



# Composite sepiolite/chitosan layer-by-layer coated flexible polyurethane foams with superior mechanical properties and energy absorption

Wenfei Ji<sup>a</sup>, Qicheng Zhang<sup>b,\*</sup>, Fernando Alvarez-Borges<sup>c</sup>, Guanjie Yuan<sup>d</sup>, Jeroen Van Duijneveldt<sup>a,\*</sup>, Wuge H. Briscoe<sup>a</sup>, Fabrizio Scarpa<sup>b</sup>

<sup>a</sup> School of Chemistry, University of Bristol, Cantock's Close, Bristol BS8 1TS, UK

<sup>b</sup> Bristol Composites Institute, University of Bristol, Bristol BS8 1TR, UK

<sup>c</sup>  $\mu$ -VIS X-ray Imaging Centre, University of Southampton, Southampton SO17 1BJ, UK

<sup>d</sup> School of Physics, University of Bristol, Bristol BS8 1TL, UK

## ARTICLE INFO

### Keywords:

Polyurethane foam  
Layer-by-layer assembly  
Energy dissipation  
Stiffness  
Damping  
Nanocomposite coatings

## ABSTRACT

Flexible polyurethane foam composites with enhanced stiffness and energy dissipation have been prepared via a facile layer-by-layer assembly approach. The composite foams consisted of naturally abundant nanoclay/chitosan multilayers (up to six) deposited onto the foam struts via dip-coating. The nanoclay/chitosan polyurethane foams were characterised using infrared spectroscopy, scanning electron microscopy, elemental mapping and  $\mu$ -CT scanning. Quasi-static mechanical compression of the foams with 6 bilayers showed a 202% increase in the stiffness and a 33% enhancement in the damping loss factor compared to the uncoated pristine foam. Vibration transmissibility tests showed that the dynamic modulus of the 6-bilayer coated foams was 3 times that of the pristine foam. Remarkably, impact tests registered a 50% decrease in the transmitted impact force of these sepiolite/chitosan layer-by-layer coated open cell polyurethane foams, demonstrating their improved energy dissipation capability compared to other nanocoated foams in open literature.

## 1. Introduction

Flexible polyurethane foams have been extensively used as cushioning materials, with a wide range of applications from furniture to automotive interiors [1], due to their intrinsic resilience, energy absorption propensity, and excellent vibration damping performance. Compared to pristine foams, flexible polyurethane foam composites (FPUFCs) show improved energy absorption and damping properties that are useful for more high-end applications, e.g. aerospace, automotive and building constructions [2,3], thanks to the additional properties provided by the filler/coating material.

PU foam composites can be prepared either by embedding filler particles into the chemicals before foaming [4] or by coating a ready-made open-cell PU foam. The latter process provides an easy approach for engineering the surface of the foam struts, allowing independent control of the foam skeleton and the coating material [5,6] without significantly affecting the physico-chemical properties of the original foams. The first coated flexible PU foam referenced in literature was prepared by Yanagi et al. [7] in 1994 to develop an artificial trachea.

Widely used on laboratory and industrial scales, the coating process depends on the specific coating materials used. In previous studies, graphene [8–11], graphene oxide [12–15] and carbon black [16] have been explored as coating materials to enhance stiffness, mechanical damping, and general dielectric properties. However, environmental footprints are always a concern for the use of carbon materials, and the external appearance (i.e., colour) of the produced foam composites is irreversibly affected by the presence of carbon. On the other hand, nanoclays have been used to prepare FPUFCs because of their attractive properties and characteristics [2]. Nanoclays are extracted from abundant natural sources and cause limited negative impacts on the environment during processing, use, and disposal [17]. The availability and ease of manufacturing guarantees the relatively low cost of nanoclays. Nanoclays also feature an intrinsic high modulus (~170 GPa), high aspect ratios (200–1000) and excellent thermal stability, making them an attractive choice as nanocoatings for foam composites [2].

To make an effective coating of the PU foams with the nanoclays, a deposition method consisting of layer-by-layer (lbl) assembly is usually chosen due to its high controllability [5], a wide range of accessible raw

\* Corresponding authors.

E-mail addresses: [qicheng.zhang@bristol.ac.uk](mailto:qicheng.zhang@bristol.ac.uk) (Q. Zhang), [j.s.van-duijneveldt@bristol.ac.uk](mailto:j.s.van-duijneveldt@bristol.ac.uk) (J. Van Duijneveldt).

<https://doi.org/10.1016/j.compstruct.2023.117419>

Received 27 March 2023; Received in revised form 25 June 2023; Accepted 26 July 2023

Available online 27 July 2023

0263-8223/© 2023 The Authors. Published by Elsevier Ltd. This is an open access article under the CC BY license (<http://creativecommons.org/licenses/by/4.0/>).

materials and processes, and the simplicity of manufacturing [18,19]. The basis of lbl assembly is an ordered formation of a stratified microstructure on the surface of a substrate. The coating can be built up, exploiting intermolecular attractions by dipping the substrate into two or more dilute reagent solutions alternately. The attractions can result from formation of chemical [20], hydrogen [21] or coordination bonds [22], or electrostatic forces [18] between adjacent layers, and between the coating layers and the substrate. In practice, a coated FPUFC can be readily prepared via electrostatic attraction from two oppositely charged coating materials, such as polyelectrolytes, nanoclays [19], and acids [18], to improve flame retardancy, gas resistance and general mechanical performance. However, a systematic study about possible energy damping improvements in lbl assembled PU foams has not been performed so far, to the best of our knowledge.

Chitosan, an amino polysaccharide from deacetylated chitin, is an abundant naturally derived biopolymer. Chitosan attracts significant research activities due to its biodegradability, biocompatibility and tenability [23–24]. It carries positive charges because of the protonation of its amino group in aqueous media, making it a frequently used reagent for lbl assembly. Sepiolite, a mineral with a composition of  $\text{SiO}_2$  and  $\text{MgO}_6$  in a 2:1 ratio, is a fibrous nano-scaled clay with zeolitic internal tunnels. This special structure gives rise to a large aspect ratio and high surface area, which accounts for its significant sorption capability. In addition, its negative surface charge allows strong complexation with positively charged polymers or surfaces. For example, sustainable sepiolite/chitosan composite films were prepared as interphase constituents for a mechanical reinforcement on a hemp/polymer biocomposite [25].

However, to the best of our knowledge, lbl assembled sepiolite/chitosan composites have not been previously used to improve the mechanical energy storage and damping in flexible polyurethane foams.

In this work, a chitosan/sepiolite nanocoating has been prepared via lbl assembly for the purpose of improving the stiffness, energy absorption, and vibration damping of flexible polyurethane foams. The morphology and chemical makeup of the treated foams have been investigated, while their mechanical behaviour and energy damping performance have been assessed via static compression, dynamic vibration, and impact tests.

## 2. Experimental section

### 2.1. Materials

Bare sepiolite (Sep, molecular formulation  $\text{Si}_{12}\text{O}_{30}\text{Mg}_8(\text{OH})_4(\text{OH}_2)_4 \cdot 8\text{H}_2\text{O}$ ), with a nanorod shape of 20–100 nm in diameter and 0.2–1  $\mu\text{m}$  in length, was obtained from Sigma-Aldrich Co. Chitosan (CS, molecular weight  $3 \times 10^5 \text{ g mol}^{-1}$ ) was purchased from Sigma-Aldrich, and polyacrylate acid (PAA, 230,000  $\text{g/mol}$ , 25% in water) from BDH Chemicals Ltd. Ultrapure water with a resistivity of 18  $\text{M}\Omega \text{ cm}$  was obtained from a Milli-Q Plus system from Millipore and used for cleaning and solution preparation. Open-cell flexible polyurethane foams (PUFs, apparent density  $28.6 \text{ kg m}^{-3}$ ) were supplied by SM Upholstery Ltd. Cardiff. All materials were used as received unless otherwise stated.

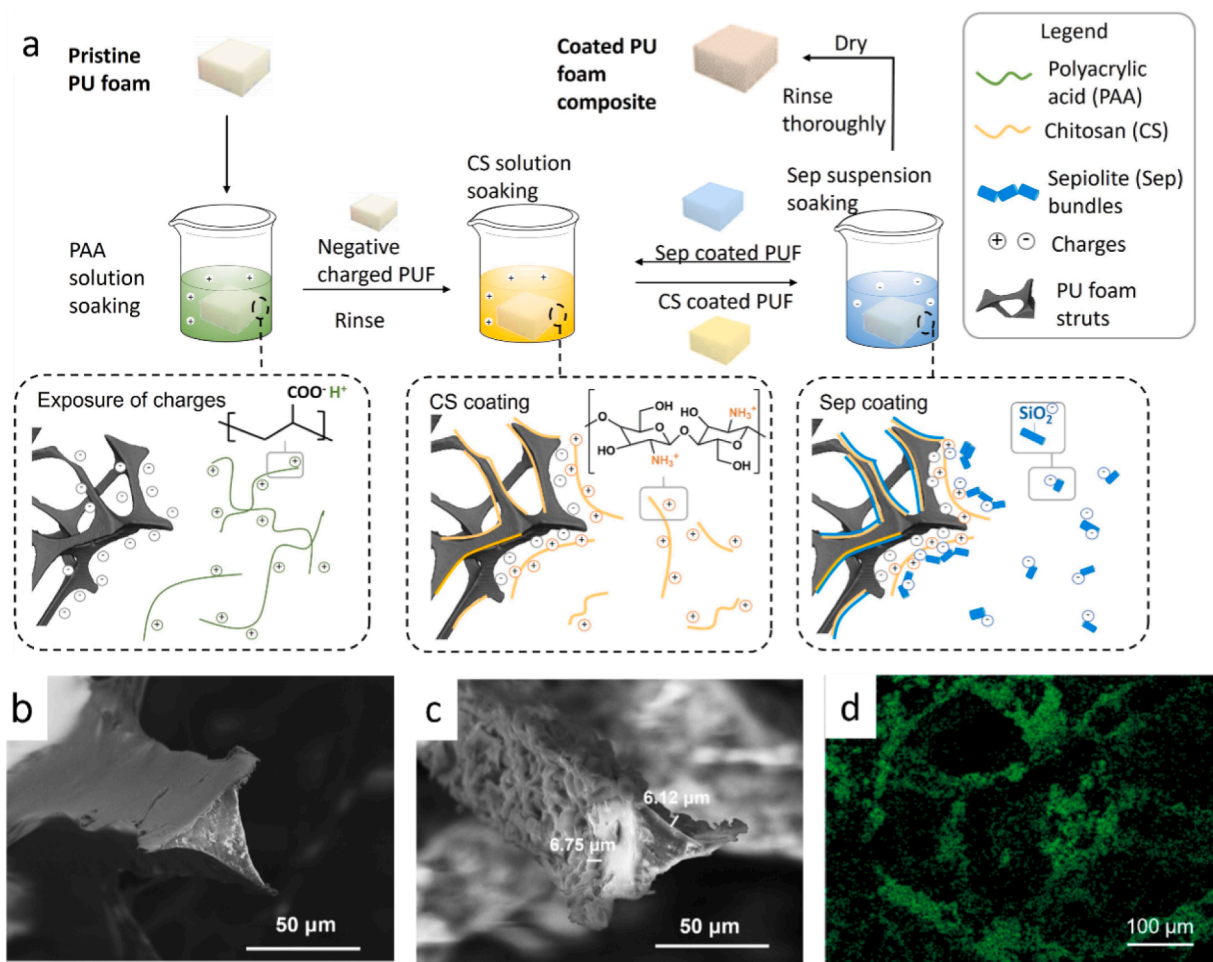


**Fig. 1.** Layer-by-layer assembly of CS/Sep coatings onto the PU foam cubes (a); SEM images of pristine PU foam (b) and the 6 bls (c); elemental distribution of silicone (d) for the 6 bls.

## 2.2. Methods

The lbl assembly method was based on previous work [26] with a few adjustments. The procedure of CS/Sep coatings is shown in Fig. 1 (a) with the details supplied in the Supporting Information. The foam samples with a size of  $30 \times 30 \times 15$  mm were individually coated via dipping into CS and Sep solutions sequentially until a designated number of layers had been applied. The coating produced after each CS and Sep cycle was denoted as a bilayer (bl), therefore the coated foams were marked as 0, 2, 4 and 6 bilayers according to the coating cycles. In Fig. 1 (b) and (c), the foam with 6 bilayers (6 bls) shows a thick coating with a thickness of 6 – 7  $\mu\text{m}$ , making a strong shell to the foam strut and protecting the flexible skeleton. The distribution of Silicon in Fig. 1 (d) proves that the clays were distributed around the PU skeleton.

## 2.3. Characterisation

Details of the characterisation and the calculation of mechanical parameters are given in Supporting Information. Fourier transform Infrared (FTIR) spectra were recorded using a PerkinElmer FT-IR Spectrometer with an attenuated total reflection (ATR) accessory. Samples were tested under the resolution of  $1 \text{ cm}^{-1}$  with 4 scans in the wavenumber range  $4000$  to  $600 \text{ cm}^{-1}$ . Thermogravimetric Analysis (TGA) were performed using a TA Q500 thermal gravimetry system. All samples were between 3 mg and 6 mg and tested in a nitrogen atmosphere, over a temperature range from  $25 \text{ }^\circ\text{C}$  to  $800 \text{ }^\circ\text{C}$  at a ramp rate of  $10 \text{ }^\circ\text{C min}^{-1}$ . Scanning electron microscopy (SEM) micrographs were taken using a Joel IT300 SEM with a resolution of 5 nm and was used jointly with energy dispersive spectroscopy (EDS). The 3D topology of the samples has been obtained using  $\mu$ -CT scanning and processed in Avizo 2019. A Zeiss Xradia 160 kVp Versa 510 scanner was used for small scanning regions ( $1.3 \times 1.3 \times 1.3$  mm), while a modified 225 kVp Nikon/Xtek HMX microfocus scanner was used for general overviews of the samples (scanning region of  $10 \times 10 \times 10$  mm).

In all mechanical tests, five identical samples were evaluated for each group, and used to extract the average and standard deviation, the latter shown in the plots as error bars. The foam samples were placed in a chamber with constant relative humidity of 52% for at least 48 h. The quasi-static compression tests were performed according to ISO604:202 using a Shimadzu universal test machine with a 1 kN load cell. The foam samples were compressed from the top surface at a rate of  $1 \text{ mm min}^{-1}$  until a maximum strain of 20% while the fifth cycle was recorded for analysis because of the Mullins effect [27]. The stress relaxation tests have been carried out at a stroke rate of  $2 \text{ mm s}^{-1}$ , with a constant strain of 30% and testing time of 5 min. In the case of creep tests, the samples were compressed at a rate of  $1 \text{ N s}^{-1}$ , until the compression force reached 5 N. The force was then kept constant for 5 min. The mechanical behaviour of coated foams during vibration was evaluated using a transmissibility test rig [27] (Fig. S1). The samples were fixed and

vibrated vertically with a seismic excitation. A custom-built drop tower rig as designed by Zhang et al. [28] (Fig. S2) for soft and porous materials has been used to characterise the impact properties of these foams, with impact energy 0.2 J and 0.4 J adjusted by the height of the drop mass.

## 3. Results and discussion

### 3.1. Chemical makeup and thermal stability of CS/Sep coatings on PU foams

FTIR was applied to chemically determine the coating layers onto the foam samples. Fig. 2 (a) shows the infrared spectra of Sep, CS and polyurethane foam in this work before and after treatment. For bare sepiolite, the Si-O coordination bands at  $1210$ ,  $1014$  and  $978 \text{ cm}^{-1}$  were formed because of the Si-O vibrations [29]. Chitosan shows characteristic signals at  $1151 \text{ cm}^{-1}$  and  $1307 \text{ cm}^{-1}$  due to C-N antisymmetric stretching [30] and C-H in the ring [31], respectively. For pristine polyurethane, the intense bands at  $1375$  and  $1583 \text{ cm}^{-1}$  are attributed to the C-N stretching vibration and N-H deformation, respectively [32]. All those signals can be seen for 4 bls coated foam samples. It proves the successful deposition of both sepiolite and chitosan onto the foams without any breakage of the polyurethane chemical structure itself. The results from FTIR show the specific bands of chitosan, sepiolite and polyurethane, with no other new absorption band appearing in the spectrum. This indicates a physical nature in the polyurethane – CS/Sep coating interactions and in the interactions between the coating layers. Fig. 2 (b) shows the TGA results of all the samples. The PU foam and the composites showed two thermal degradation stages at  $270 \text{ }^\circ\text{C}$  and  $378 \text{ }^\circ\text{C}$ , because of the release of the diisocyanate and the pyrolysis of the polyether chain, respectively [26]. This demonstrates that the pyrolysis of polyurethane was not affected by the sepiolite coatings. The thermal stability of the coated PU foams was however improved, resulting in an increased amount of residues at  $750 \text{ }^\circ\text{C}$  (~14 % of the 6 bls, compared to ~2% of the pristine foam).

### 3.2. 3D morphology of CS/Sep coatings on PU foams

The morphology obtained from the CT scanning of the pristine foam and the one coated with 6 bls in a scanned cube with a side length of 1.3 mm is shown in Fig. 3 (a) and (b), respectively. It is evident that the coating layers were deposited and attached onto the foam ribs, making the rib surfaces rough, but without disrupting or destructing the original structure of the foam. The orientation and topologic parameters of the foam ribs were obtained from a skeletonised model (Fig. 3 c) using the methodology described in previous work [33]. Fig. 3 (d) shows an inclination of the foam ribs along the direction 3 (indicated as point B), while a lower number of ribs is oriented along the direction 1 (point A), or direction 2. The original orientation of the foam ribs due to the

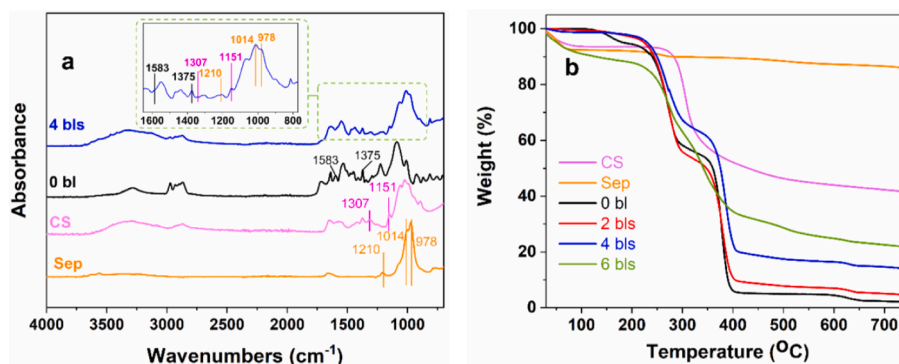
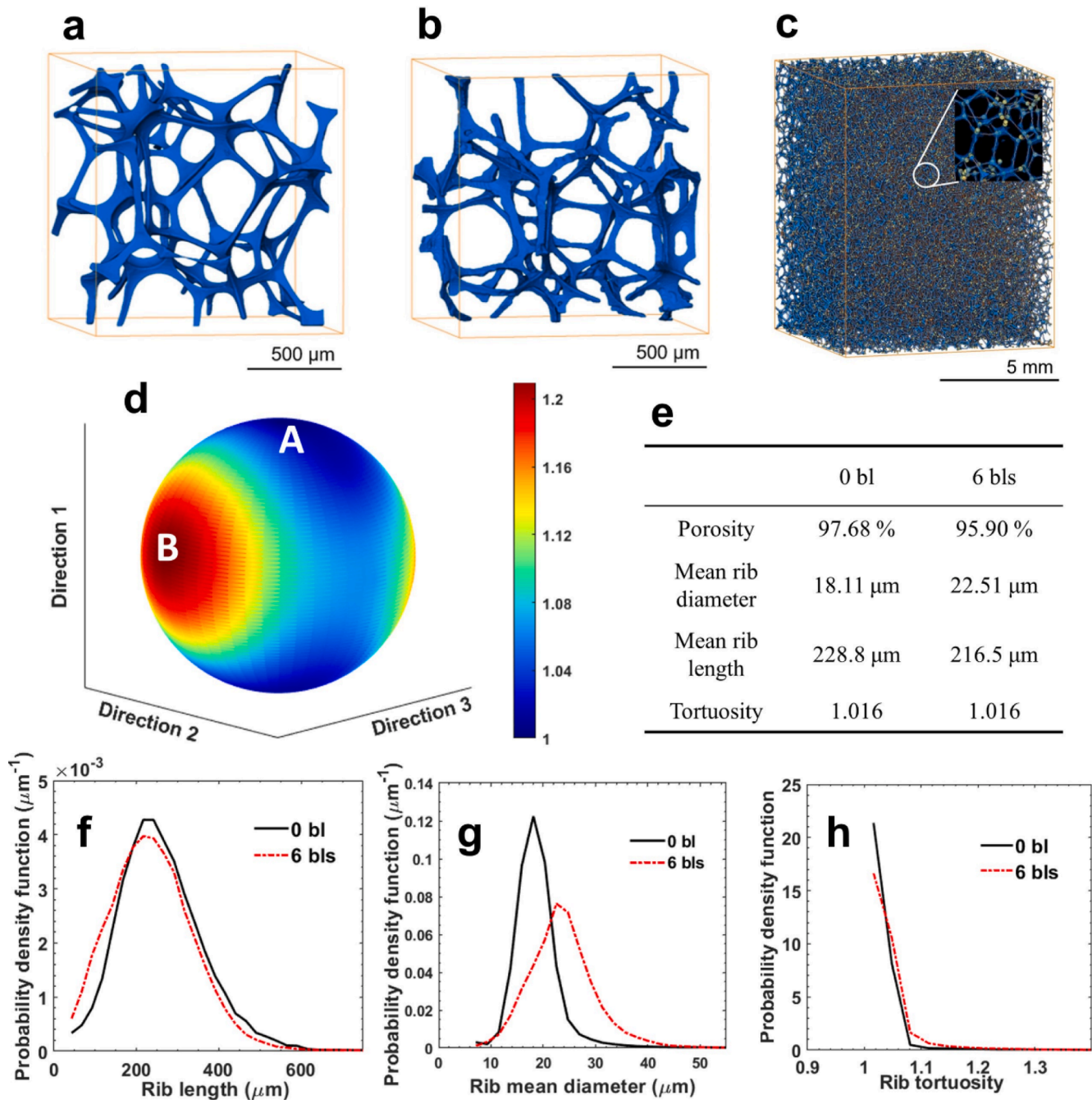


Fig. 2. (a): FTIR spectra of sepiolite, chitosan, PU foam (0 bl), and PU foam coated with 4 layers of the composite (4 bls). The inset shows the enlarged view for the 4 bls in the wavenumber range  $1500 - 800 \text{ cm}^{-1}$ . (b): TGA curves of sepiolite, chitosan and PU foam samples.



**Fig. 3.** 3D topology and morphology of the cross sections for pristine PU foams (a); foams coated with 6 bls (b); the processed and skeletonised models of 6 bls (c); the orientation distribution map of 6 bls (d); the main topology parameters (e); a probability density function versus rib length (f); mean diameter (g); and tortuosity (h) for the PU foam with 0 and 6 bls.

industrial manufacturing processes [27] was virtually unchanged by the presence of the coatings.

The statistical distributions of the length, diameter and tortuosity of the foam ribs of 0 bl and 6 bls from that post-processing are presented in Fig. 3 (f), (g) and (h), respectively, with the key parameters listed in Fig. 3 (e). The porosity, defined as the ratio of the air volume to the sample volume, indicates that the foam volume was overwhelmingly occupied by air (97.68% of 0 bl and 95.90% of 6 bls). The sepiolite–chitosan coatings did not compromise the original porous and lightweight topology of the foams. The 6 bls showed a similar rib length to the pristine foam, while a slight increase of the rib diameter due to the coating materials. The tortuosity was calculated by dividing the rib

length with the distance between the two ends of the rib [33]. For both foam samples, the ribs were only mildly bent (i.e., with a tortuosity of 1.016 - slightly above 1). In summary, the coatings did not appear to have altered the baseline pristine foam structure.

### 3.3. Mechanical performance of CS/Sep coated foams

#### 3.3.1. Quasi-static compression tests for CS/Sep coated foams

Fig. 4 (a) and (b) shows the stress vs strain load curves and tangent modulus ( $E_{tan}$ ) from the quasi-static compression of the pristine and coated samples, along with the key parameters listed in Table 1. The Young's modulus  $E$ , calculated as the slope of the fitted stress–strain line

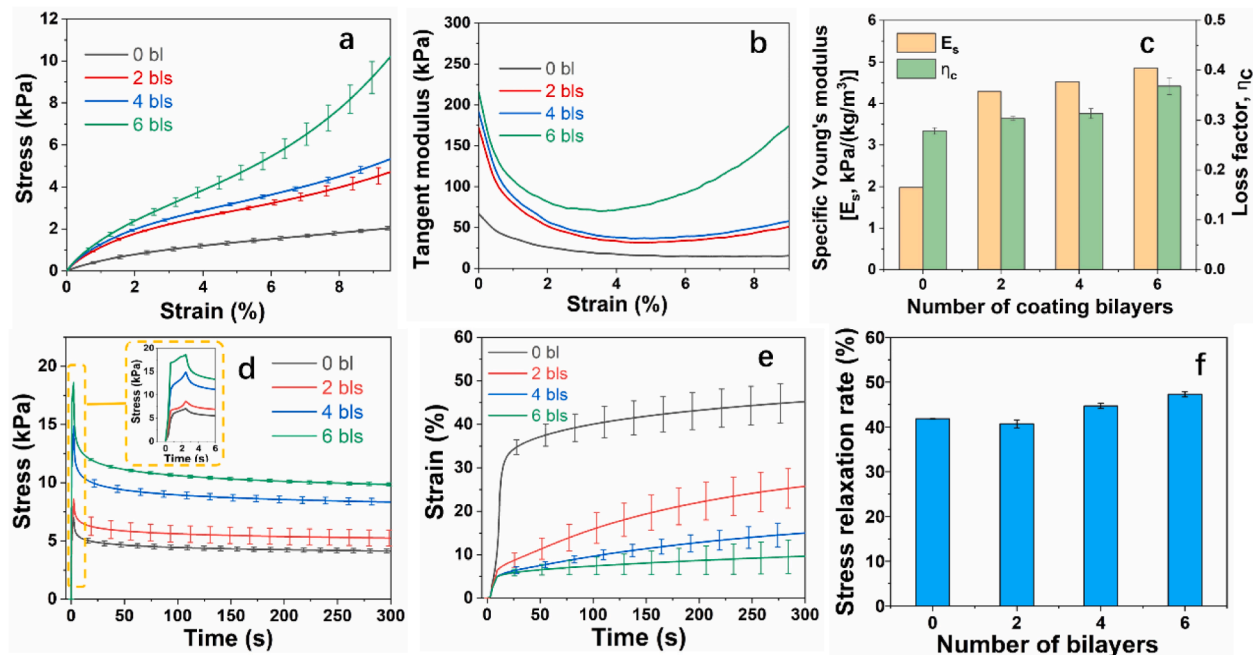


Fig. 4. The mechanical and quasi-static energy dissipation properties of the PU foam coated with 0, 2, 4 and 6 bls. The stress vs strain load curves (a); tangent modulus (b); specific Young's modulus and loss factor (c); stress relaxation curves (d); creep test results (e); and stress relaxation rates (f).

Table 1

Physical and mechanical characterisation results for the foam samples with 0, 2, 4 and 6 bls from the quasi-static tests.

Samples	Weight of the CS/Sep coatings (mg)	Density, $\rho$ (kg/m <sup>3</sup> )	Young's Modulus, $E$ (kPa)	$\Delta W$ (J/m <sup>3</sup> )	Mean crushing force, $MCF$ (N)	Specific energy absorption, $SEA$ (J/kg)
0 bl	–	28.0 ± 1.2	55.4 ± 6.8	8.3 ± 1.5	7.0 ± 0.4	53.0 ± 3.5
2 bls	41.8 ± 5.5	31.1 ± 0.5	133.6 ± 7.9	24.3 ± 1.6	8.2 ± 0.2	61.1 ± 2.3
4 bls	71.6 ± 7.7	33.3 ± 0.7	150.5 ± 5.6	25.3 ± 1.0	8.6 ± 0.2	60.8 ± 1.4
6 bls	89.1 ± 17.6	34.6 ± 1.6	167.5 ± 8.1	23.5 ± 1.6	9.4 ± 0.6	62.5 ± 3.0

within 0–0.5% strain, is increased by 78.2 kPa from the 0 to 2 bls foams; this increase is more pronounced compared to that between the 2 and 4 bls, or between the 4 and 6 bls specimens. Similarly, the specific Young's modulus  $E_s$  increased significantly in the samples coated with 0 to 2 bilayers, then gradually increased above 2 bls (Fig. 4 c). A significant increase of the  $E_{tan}$  can also be observed after coating with more layers, with a zero-strain modulus of 6 bls at ~215 kPa compared to ~65 kPa of the untreated foams. For the 0, 2 and 4 bls, the  $E_{tan}$  shows a drop with the strain until 4%, followed by a plateau until 8% strain, exhibiting a nonlinear viscoelastic behavior [34]. The  $E_{tan}$  of 6 bls, however, starts to rise at ~3% strain and increases due to increased stiffness caused by densification of the cell structures. For the case of 6 bls, the coating layers thicken the foam ribs, and this facilitates the mutual contact and triggers densification at lower strains, compared to foams coated with fewer nanoclay layers.

The  $\Delta W$  (energy dissipated) and  $\eta_c$  (the loss factor) show a gradually improved ability in terms of energy dissipation of the foam composite until 6 bilayers were coated. Two coating bilayers largely contributed to an enhancement of  $\Delta W$  from 8.3 J/m<sup>3</sup> to 24.3 J/m<sup>3</sup>, which increased to 25.3 J/m<sup>3</sup> when 2 more layers were added. The increment of energy dissipated began to drop for samples with 6 bls. Meanwhile, the loss factor varied from 0.28 to 0.30 with the presence of 2 bilayers, while a slight increase of 0.01 with additional 2 or more bilayers was observed, as shown in Fig. 4 (c). The energy can be dissipated via two main mechanisms: the deformation of the foam ribs (e.g., bending and buckling), and the friction between coating layers or the coating-PU

interface. For the 2 bls and 4 bls, the tight combination between the coating layer and the foam struts along with sepiolite and chitosan contributes to a higher damping performance when the foam is deformed by bending and buckling. However, for the 6 bls, the energy is mainly dissipated by the compression and shear of the foam ribs. This change of deformation decreases the local strain in the ribs and then reduces the effect of the energy damping [8], which causes only a slight improvement of the loss factors  $\eta_c$  between the 4 bls and the 6 bls specimens.

The mean crushing force ( $MCF$ ) shifted from the pristine foam (7.0 N) to 6 bls (9.4 N), indicating a better capability for resisting crushing loads with the presence of the coatings. The values of the specific energy absorption ( $SEA$ ) also show an effective improvement of the damping for the coated samples, suggesting that the significant energy absorption effect is facilitated by the coating - PU foam interactions, rather than the inter-layer interactions.

As a vital role in determining the load bearing capability of polymers, stress relaxation and creep performance are tested, as shown in Fig. 4 (d) and (e), respectively. In Fig. 4 (f), the stress rate  $R_s$  slightly decreased when the foam was coated with 2 bilayers, and this is due to the stiffening effect from the added nanoclays. The rate then increased with the presence of more coating layers because gradual slippage occurring between the nanoclay layers tends to cause more deformation of the foam composite under continuous loading. The sample with 6 bilayers underwent the largest interface slip, causing the highest  $R_s$ . In the case of creep (Fig. 4 e), the coated foam samples only exhibited a small creeping

deformation ( $\sim 5\%$  strain) during the first 20 s due to the coating-stiffened skeletons, unlike the pristine foam that deformed rapidly, showing a sharp increase (35% strain) at the beginning of the test. These coatings rigidify the foams which leads to a lower deformation with time; this effect is enhanced by the presence of more coating layers. The foam with 6 bls underwent densification when the strain was above 6% (see Fig. 4 a), which improved the stiffness and caused the lowest creep amongst all of the samples.

### 3.3.2. Dynamic vibration and transmissibility tests for CS/Sep coated foams

Commonly used for load bearing applications such as automotive seatings, PU foam cushions are now designed for high levels of damping to increase ride comfort and safety [35]. This leads to a better absorption of kinetic energy and a more effective transformation into heat during vibration. The coated foam samples have been tested using a custom-built transmissibility test rig [27] (shown in Fig. S1) with the transfer functions shown in Fig. 5 (a). Compared to pristine PU foams ( $\sim 52$  Hz), foams with 2 and 4 bilayers showed the highest resonance frequency ( $\sim 78$  Hz), with the 6 bls sample showing a maximum frequency of  $\sim 100$  Hz. This is because the foam skeleton is strongly supported by the clay-chitosan coatings, which stiffen the composite and increase the resonance frequency.

The dynamic modulus  $E_d$  (also called the storage modulus), loss factors  $\eta_d$  and loss modulus  $E_l$  of the foams coated with 0, 2, 4 and 6 bls

have been identified from the resonance and transmissibility amplitudes according to the equations in Supplementary Information, as shown in Fig. 5 (b), (c) and (d). Five types of top masses were attached on the top of the samples to modify the resonances of the systems. The  $E_d$  of the foams tended to increase first, and then plateaued at higher frequencies. This is because the smaller resonance frequencies correspond to larger top masses, which provide larger pre-compression levels and greater dynamic deformations during the transmissibility test. According to the results from the quasi-static tests (Fig. 4), the larger deformation also led to a smaller modulus. This can be also verified by evaluating the results with different base accelerations (see Fig. S3 of the Supporting Information). The shift of the  $E_d$  at higher frequencies is noticeable, with higher values for more coating layers due to the stiffening effect from the clay coatings. In Fig. 5 (b), the maximum  $E_d$  values are 0.11 MPa, 0.22 MPa, 0.25 MPa and 0.34 MPa for the 0, 2, 4 and 6 bls foams, respectively, much larger than their corresponding static Young's modulus (Table 1). This is partially due to the pneumatic force exerted on the porous material and the higher strain rates during the dynamic tests [27]. Furthermore, the smaller dynamic strain at higher resonance frequencies with a small top mass could partially lead to the enhancement of the  $E_d$ , compared with the quasi-static test results.

The loss factor  $\eta_d$  of the samples is shown in Fig. 5 (c), indicative of the ability of the foam to dissipate vibration energy. For the PU foam system used in this work, the vibration energy can be dissipated through different mechanisms: (1) coating-foam interfacial friction, (2) coating-

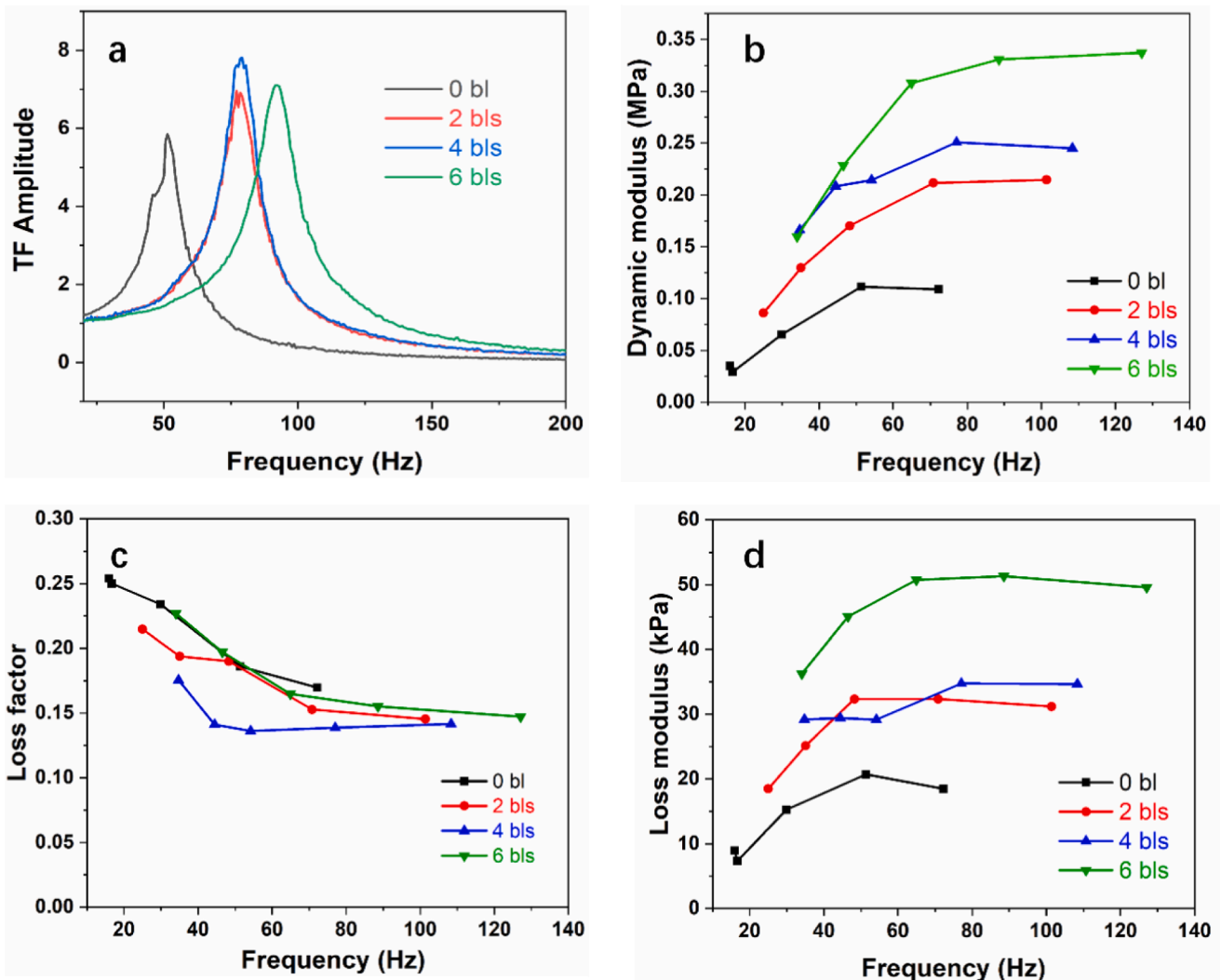


Fig. 5. The transfer functions (a), dynamic modulus (b), loss factor (c), and loss modulus (d) of samples coated with 0, 2, 4 and 6 bls at a base acceleration of 0.69 g.

coating interfacial friction, (3) deformation and viscosity of the PU foam structure, and (4) pneumatic damping of the air. Although the interfacial sliding between coatings can help to enhance the energy dissipation of the foam [8,9], the  $\eta_d$  of the coated samples was slightly lower than the 0 bl. This is because the small stiffness of the 0 bl leads to the larger dynamic deformation compared with the coated foam, which results in larger damping from the viscoelastic load deformation of the PU and the pneumatic force provided by the airflow. The damping enhancement introduced by the micro friction of the coating layer cannot compensate for the reduction in damping caused by a larger stiffness and a smaller deformation. The  $\eta_d$  of the different foams all increased with the decreasing resonance frequency. The low resonance frequency corresponds to a heavier top mass, larger precompression, and larger dynamic deformation, which introduces higher damping from the viscosity of the PU of the foam and airflow effects.

The loss modulus  $E_l$  (shown in Fig. 5 d) demonstrates the damping behaviour and the overall energy dissipation capability of the material under cyclic loading [36]. Due to the larger  $E_d$  as well as the moderate  $\eta_d$ , the sample with 6 bls exhibited the greatest  $E_l$  values (51.3 kPa at 88.5 Hz) among all the samples. The sample coated with 2 and 4 bls showed similar  $E_l$ , while the pristine foam had the lowest possible  $E_l$  value. The pristine foam, even though it was heavily deformed during the tests, ultimately exhibited the worst damping performance due to the lack of friction and insufficient intrinsic stiffness.

It is worth mentioning that, with the increase of the base amplitude, the levels of vibration increase. These can lead to the potential triggering of microcracks in the coatings of the struts. The presence of cracks makes the composite softer, leading to a decrease of the resonance frequency. The difference caused by the base acceleration level becomes larger in the case of the coated foams, which marks the presence of a significant nonlinearity of the system. The base acceleration also affects the  $E_d$  and  $\eta_d$  as discussed in detail in the [Supporting Information](#).

### 3.3.3. Impact behaviour of the CS/Sep coated PU foams

Energy-absorbing PU foams are widely used in seat cushions, bumpers, and side impact protection systems [37]. A method to evaluate the energy absorption properties under impact is to use a drop-tower experimental rig developed in previous work [28]. During the drop-tower tests, the kinetic energy was kept constant (maximum 0.4 J in this work). The reaction peak force represents the maximum force transmitted through the impacted foam samples. As shown in Fig. 6 (a) and (b), the coatings provided a significant reduction in the impact force compared to the pristine foam, with two bilayers already providing a 24% attenuation for an impact of 0.2 J, and an even larger 36% attenuation in the case of 0.4 J. The presence of 6 bls led to a  $\sim$ 50% reduction in the peak force compared to the pristine foam, for both levels of kinetic energy tested. The clay-chitosan coating systems used in this work can change the impact mechanical behaviour of the foams in two ways. First,

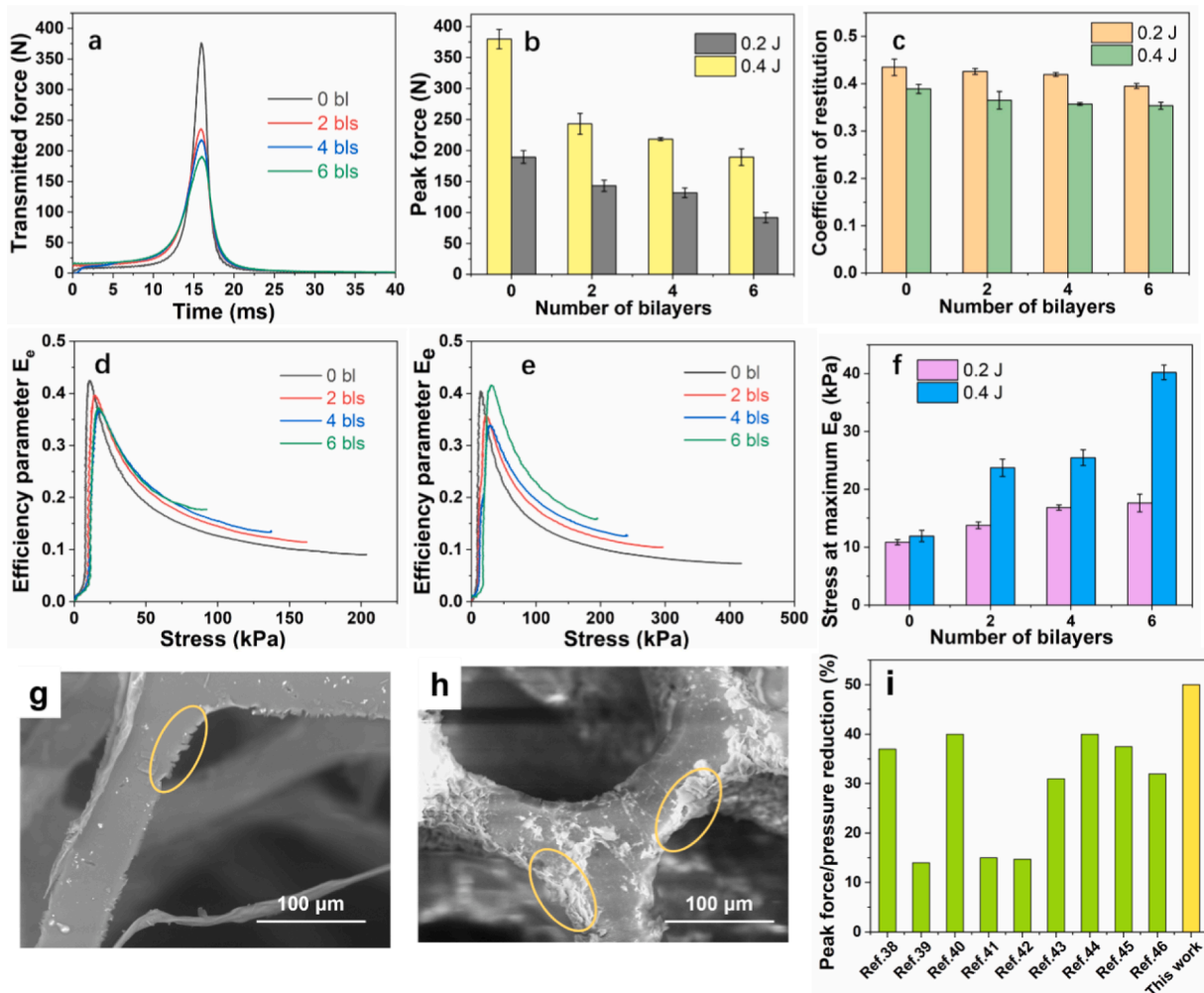


Fig. 6. Impact test results for the PU foam samples coated with 0, 2, 4 and 6 bilayers. (a) Transmitted force at 0.4 J; (b) peak force values; (c) coefficient of restitution  $e$  for each group of foams; efficiency parameters  $E_e$  for energy groups of (d) 0.2 J and (e) 0.4 J; and (f) stress at the peak of the efficiency parameters for each foam group; SEM images of (g) pristine foam and (h) the 6 bls after five repeated impacts with 0.2 J. (i): a comparison of the reduced peak force/pressure of the sepiolite chitosan nanocoated foams described in this work and analogous values from other studies.

materials dissipate energy mainly at the plateau stage of the stress–strain loops [37], and the foams with higher apparent density (cf. Table 1) usually reach a plateau at larger stresses, leading to an increased impact energy absorption. Secondly, the micro friction of the coating layers helps enhance the impact energy dissipation. On the other hand, the coatings stiffen the foam skeletons, so that they are not as vulnerable to the external impact force as the bare PU foam scaffold. Therefore, even the final dissipated energy  $W_{final}$  is essentially the same for all samples (Fig. S5), the stiffer coated foams showed a reduction in the transient absorbed energy  $W_{max}$ .

The coefficient of restitution  $e$  (Equation S12) indicates essentially the level of dissipation of the kinetic energy during the impact. As illustrated in Fig. 6 (c), the  $e$  decreased with the number of coatings and it was lower for the 0.4 J impact force results, while it showed a slightly more erratic trend between the coated foams with 0.2 J. This means that more impact energy has been dissipated in the foams coated with more layers with higher energy. The energy dissipation by the coated PU foam mainly originates from: (1) the viscoelastic deformation of the foam skeletons, (2) the pneumatic damping of the airflow [37], (3) the friction between coating layers and the PU foam struts, and (4) the friction between coating layers. Therefore, the coated foams showed an improved impact energy dissipation capacity and lower  $e$  because of the micro frictions present between the coating layers.

An efficiency parameter  $E_e$  (cf. Equation S11) is shown in Fig. 6 (d) and (e) as a function of the stress. Each curve shows a maximum  $E_e$  at a specific stress, which defines the optimum usage of the material for impact applications [28]. In Fig. 6 (f), all the PU foam samples in this work showed a maximum  $E_e$  at a similar stress (between 10 and 20 kPa) in the 0.2 J group, while the stress increased for the 0.4 J group (between 11 to 40 kPa). Compared to uncoated foams, the coated ones showed the peak at higher stresses, with their efficiency curves gradually softening. Therefore, the coating materials enhanced the optimum stress range for foams designed to absorb impact energy.

The morphology of the pristine foam and that with 6 bls after five repeated impacts are compared in Fig. 6 (g) and (h). As shown by the yellow circles, the edges of the uncoated foam appear abraded. The coating materials however still bonded to the foam struts, which helped supporting and stiffening the PU skeleton. Therefore, the foams were protected from being damaged by the impact, and the energy damping was improved. It results in a similar increase in the impact force between the uncoated and 6 bls samples, shown in Fig. S6. Fig. 6 (i) illustrates the reduction of the peak force or pressure from impact tests described in previous studies [38–46]. For example, Lu et al. [38] fabricated a hierarchical porous composite using PU foams, carbon materials and polymer matrix that provided a transmitted impact force reduced by 37% compared to the untreated foam. Hosur et al. [41] prepared novel sandwich panels with 1 wt% clay modified PU foam cores, resulting in a 15% reduction in impact peak force. A shear thickening gel (STG)/PU foam composites were made by Liu et al. [42]. With 30% STG, the impact force showed ~15% decrease compared to that of the pristine PU foam. Moreover, Yang et al. [45] created a silica aerogel incorporated PU foam composite, which achieved a 37% reduction in the peak impact force with 15% aerogels into the foam structure. The coated PU foam composite prepared in this work reduced the impact force more effectively compared to other PU foam composites described in the literature and showed an excellent energy damping behaviour.

#### 4. Conclusion

In this work, a nanoclay/PU foam composite has been designed and successfully fabricated via facile layer-by-layer assembly technology. The chitosan/sepiolite coatings reinforced the PU foam skeleton, resulting in overall enhanced quasi-static and dynamic mechanical performance, as assessed by the comprehensive mechanical tests. Both the Young's modulus and the dynamic modulus of the modified foams were three times that of untreated PU foams, and the increased loss

modulus along with the decreased impact force showed enhanced cushioning effect of the coated PU foam composites. These improvements are attributed to the interfacial friction, stiffening, and augmented resistance of deformation of the composite by the presence of the coating layers. Impact peak forces reductions were also significantly improved up to a factor of 3, compared to other composite foam systems described in the literature. The findings of this work provide a simple and effective method for PU foam composites preparation for enhanced mechanical and damping performances in PU foam applications. Whilst in this work we have focused on the quasi-static compression test, it will also be interesting to perform cyclic compression tests, e.g. for 100 cycles as reported in [10,47,48].

#### CRediT authorship contribution statement

**Wenfei Ji:** Conceptualization, Methodology, Data curation, Investigation, Software, Writing – original draft, Writing – review & editing. **Qicheng Zhang:** Methodology, Data curation, Investigation, Software, Writing – review & editing. **Fernando Alvarez-Borges:** Methodology, Software. **Guanjie Yuan:** Data curation, Software. **Jeroen Van Duijneveldt:** Conceptualization, Writing – review & editing, Supervision, Funding acquisition. **Wuge H. Briscoe:** Conceptualization, Writing – review & editing, Supervision, Funding acquisition. **Fabrizio Scarpa:** Conceptualization, Writing – review & editing, Supervision, Funding acquisition.

#### Declaration of Competing Interest

The authors declare that they have no known competing financial interests or personal relationships that could have appeared to influence the work reported in this paper.

#### Data availability

Data will be made available on request.

#### Acknowledgement

WJ would like to thank the China Scholarship Council and the Faculty of Science of the University of Bristol for supporting this work through a scholarship to WJ.  $\mu$ -CT scanning was performed by the National Research Facility for Lab X-ray CT (NXCT) at the  $\mu$ -VIS X-ray Imaging Centre, University of Southampton, through the UK Engineering & Physical Sciences Research Council (EPSRC) grant EP/T02593X/1. The author would also like to thank Dr Jean-Charles Eloi from the School of Chemistry of the University of Bristol for helping obtain the SEM results. FS would also like to acknowledge the support of the ERC-2020-AdG 101020715 NEUROMETA project.

#### Appendix A. Supplementary material

Supplementary data to this article can be found online at <https://doi.org/10.1016/j.compstruct.2023.117419>.

#### References

- [1] Alongi J, Carosio F. Flame retardancy of flexible polyurethane foams: traditional approaches versus layer-by-layer assemblies. In: Novel fire retardant polymers and composite materials; 2017. p. 171–200.
- [2] Kausar A. Polyurethane composite foams in high-performance applications: A review. *Polym Plast Technol Eng* 2018;57(4):346–69.
- [3] Pang Y, Yan X, Qu J, Wu L. Dynamic response of polyurethane foam and fiber orthogonal corrugated sandwich structure subjected to low-velocity impact. *Compos Struct* 2022;282:114994.
- [4] Caglayan C, Osken I, Atalp A, Turkmen H, Cebeci H. Impact response of shear thickening fluid filled polyurethane foam core sandwich composites. *Compos Struct* 2020;243:112171.
- [5] Richardson JJ, Björnalm M, Caruso F. Technology-driven layer-by-layer assembly of nanofilms. *Science* 2015;348(6233).

- [6] Li C, Ye H, Ge S, Yao Y, Ashok B, Hariram N, et al. Fabrication and properties of antimicrobial flexible nanocomposite polyurethane foams with in situ generated copper nanoparticles. *J Mater Res Technol* 2022;19:3603–15.
- [7] Yanagi M, Kishida A, Shimotakahara T, Matsumoto H, Nishijima H, Akashi M, et al. Experimental study of bioactive polyurethane sponge as an artificial trachea. *ASAIO J* 1994;40(3). M412-M418.
- [8] Lu W, Qin F, Zhang Q, Remillat C, Wang H, Scarpa F, et al. Engineering foam skeletons with multilayered graphene oxide coatings for enhanced energy dissipation. *Compos Part A Appl Sci Manuf* 2020;137:106035.
- [9] Lu W, Qin F, Wang Y, Luo Y, Wang H, Scarpa F, et al. Engineering graphene wrinkles for large enhancement of interlaminar friction enabled damping capability. *ACS Appl Mater Interfaces* 2019;11(33):30278–89.
- [10] Cura F, Sesana R, Zhang X, Scarpa F, Lu W, Peng H. Stiffness, Energy Dissipation, and Hyperelasticity in Hierarchical Multilayer Composite Nanocoated Open-Cell Polyurethane Foams. *Adv Eng Mater* 2019;21(12):1900459.
- [11] Zhang X, Scarpa F, McHale R, Limmack A, Peng H. Carbon nano-ink coated open cell polyurethane foam with micro-architected multilayer skeleton for damping applications. *RSC Adv* 2016;6(83):34–41.
- [12] Qiang F, Hu L, Gong L, Zhao L, Li S, Tang L. Facile synthesis of super-hydrophobic, electrically conductive and mechanically flexible functionalized graphene nanoribbon/polyurethane sponge for efficient oil/water separation at static and dynamic states. *Chem Eng J* 2018;334:2154–66.
- [13] Wu Q, Gong L-X, Li Y, Cao C-F, Tang L-C, Wu L, et al. Efficient flame detection and early warning sensors on combustible materials using hierarchical graphene oxide/silicone coatings. *ACS Nano* 2018;12(1):416–24.
- [14] Yu Z-R, Mao M, Li S-N, Xia Q-Q, Cao C-F, Zhao Li, et al. Facile and green synthesis of mechanically flexible and flame-retardant clay/graphene oxide nanoribbon interconnected networks for fire safety and prevention. *Chem Eng J* 2021;405:126620.
- [15] Ma Z, Zhang J, Liu L, Zheng H, Dai J, Tang L-C, et al. A highly fire-retardant rigid polyurethane foam capable of fire-warning. *Compos Commun* 2022;29:101046.
- [16] Ghosh S, Ganguly S, Remanan S, Mondal S, Jana S, Maji PK, et al. Ultra-light weight, water durable and flexible highly electrical conductive polyurethane foam for superior electromagnetic interference shielding materials. *J Mater Sci – Mater Electron* 2018;29(12):10177–89.
- [17] Wu F, Pickett K, Panchal A, Liu M, Lvov Y. Superhydrophobic polyurethane foam coated with polysiloxane-modified clay nanotubes for efficient and recyclable oil absorption. *ACS Appl Mater Interfaces* 2019;11(28):25445–56.
- [18] Carosio F, Alongi J. Ultra-fast layer-by-layer approach for depositing flame retardant coatings on flexible PU foams within seconds. *ACS Appl Mater Interfaces* 2016;8(10):6315–9.
- [19] Liu Q, Gao S, Zhao Y, Tao W, Yu X, Zhi M. Review of layer-by-layer self-assembly technology for fire protection of flexible polyurethane foam. *J Mater Sci* 2021;56(16):9605–43.
- [20] Bergbreiter DE, Chance BS. “Click”-based covalent layer-by-layer assembly on polyethylene using water-soluble polymeric reagents. *Macromolecules* 2007;40(15):5337–43.
- [21] Kim B, Park SW, Hammond PT. Hydrogen-bonding layer-by-layer-assembled biodegradable polymeric micelles as drug delivery vehicles from surfaces. *ACS Nano* 2008;2(2):386–92.
- [22] Shimazaki Y, Nakamura R, Ito S, Yamamoto M. Molecular weight dependence of alternate adsorption through charge-transfer interaction. *Langmuir* 2001;17(3):953–6.
- [23] Michel SES, Rogers SE, Briscoe WH, Galan MC. Tunable Thiol-Ene Photo-Cross-Linked Chitosan-Based Hydrogels for Biomedical Applications. *ACS Appl Bio Mater* 2020;3(11):8075–83.
- [24] Michel SS, Kilner A, Eloi J-C, Rogers SE, Briscoe WH, Galan MC. Norbornene-Functionalized Chitosan Hydrogels and Microgels via Unprecedented Photoinitiated Self-Assembly for Potential Biomedical Applications. *ACS Appl Bio Mater* 2020;3(8):5253–62.
- [25] Battezzozze D, Frache A, Carosio F. Sustainable and high performing biocomposites with chitosan/sepilolite layer-by-layer nanoengineered interphases. *ACS Sustain Chem Eng* 2018;6(8):9601–5.
- [26] Pan H, Wang W, Pan Y, Song L, Hu Y, Liew KM. Formation of layer-by-layer assembled titanate nanotubes filled coating on flexible polyurethane foam with improved flame retardant and smoke suppression properties. *ACS Appl Mater Interfaces* 2015;7(1):101–11.
- [27] Zhang Q, Yu X, Scarpa F, Barton D, Zhu Y, Lang Z-Q, et al. A dynamic poroelastic model for auxetic polyurethane foams involving viscoelasticity and pneumatic damping effects in the linear regime. *Mech Syst Signal Process* 2022;179:109375.
- [28] Zhang Q, Scarpa F, Barton D, Zhu Y, Lang Z-Q, Zhang D, et al. Impact properties of uniaxially thermoformed auxetic foams. *Int J Impact Eng* 2022;163:104176.
- [29] Zabih A, Celik M. Interaction of pyridine derivatives with sepilolite. *J Colloid Interface Sci* 2002;251(1):33–8.
- [30] Lawrie G, Keen I, Drew B, Chandler-Temple A, Rintoul L, Fredericks P, et al. Interactions between alginate and chitosan biopolymers characterized using FTIR and XPS. *Biomacromolecules* 2007;8(8):2533–41.
- [31] Pawlak A, Mucha M. Thermogravimetric and FTIR studies of chitosan blends. *Thermochim acta* 2003;396(1–2):153–66.
- [32] Sevilla M, Valle-Vigón P, Fuertes AB. N-doped polypyrrole-based porous carbons for CO<sub>2</sub> capture. *Adv Funct Mater* 2011;21(14):2781–7.
- [33] Zhang Q, Lu W, Scarpa F, Barton D, Rankin K, Zhu Y, et al. Topological characteristics and mechanical properties of uniaxially thermoformed auxetic foam. *Mater Des* 2021;211:110139.
- [34] Zhang Q, Lu W, Scarpa F, Barton D, Lakes RS, Zhu Y, et al. Large stiffness thermoformed open cell foams with auxeticity. *Appl Mater Today* 2020;20:100775.
- [35] Shan CW, Ghazali MI, Idris MI. Improved vibration characteristics of flexible polyurethane foam via composite formation. *Int J Autom Mech E* 2013;7:1031–42.
- [36] Mead DJ. *Passive vibration control*. John Wiley & Sons; 1998.
- [37] Avasse M, Belingardi G, Montanini R. Characterization of polymeric structural foams under compressive impact loading by means of energy-absorption diagram. *Int J Impact Eng* 2001;25(5):455–72.
- [38] Lu W, Zhang Q, Qin F, Xu P, Chen Q, Wang H, et al. Hierarchical network structural composites for extraordinary energy dissipation inspired by the cat paw. *Appl Mater Today* 2021;25:101222.
- [39] Njuguna J, Michalowski S, Pielichowski K, Kayvantash K, Walton AC. Fabrication, characterization and low-velocity impact testing of hybrid sandwich composites with polyurethane/layered silicate foam cores. *Polym Compos* 2011;32(1):6–13.
- [40] Yu YH, Nam S, Lee D, Lee DG. Cryogenic impact resistance of chopped fiber reinforced polyurethane foam. *Compos Struct* 2015;132:12–9.
- [41] Hosur M, Mohammed A, Zainuddin S, Jeelani S. Impact performance of nanophased foam core sandwich composites. *Mater Sci Eng A Struct Mater* 2008;498(1–2):100–9.
- [42] Liu X, Huo J, Li T-T, Wang H, Wu L, Lin J-H, et al. Mechanical properties of a STF capsule filled flexible polyurethane composite foam. *Mater Lett* 2020;269:127580.
- [43] Pan Y-J, Lou C-W, Hsieh C-T, Huang C-H, Lin Z-I, Li C-W, et al. Nonwoven fabric/spacer fabric/polyurethane foam composites: physical and mechanical evaluations. *Fiber Polym* 2016;17(5):789–94.
- [44] Yan R, Wang R, Lou C, Huang S, Lin J. Quasi-static and dynamic mechanical responses of hybrid laminated composites based on high-density flexible polyurethane foam. *Compos B Eng* 2015;83:253–63.
- [45] Yang G, Liu X, Lipik V. Evaluation of silica aerogel-reinforced polyurethane foams for footwear applications. *J Mater Sci* 2018;53(13):9463–72.
- [46] Sharei A, Safarabadi M, Mashhadi MM, Solut RS, Haghighi-Yazdi M. Experimental and numerical investigation of low velocity impact on hybrid short-fiber reinforced foam core sandwich panel. *J Compos Mater* 2021;55(29):4375–85.
- [47] Montero Ignacio G, Raffaella S, Sebastian D, Fabrizio S. Cyclic compression behaviour of multilayered nanostructured foams: Numerical meso scale modelling and experimental validation. *Eng Fail Anal* 2023;143:106903.
- [48] Cura F, Sesana R, Scarpa F, Zhang X, Peng H. Static and dynamic behavior of PU foams with multilayer coatings. *Procedia Struct Integrity* 2019;19:388–94.